doi: 10.82124/CEAS-GNC-2026-021 CEAS-GNC-2026-021

Joint Navigation and Control Sensitivity Functions: Towards a Unified Framework for Robust Pointing Verification

Mirko Aveta AOCS Engineer, D-Orbit Spa, Fino Mornasco (CO), Italy. mirko.aveta@dorbit.space

ABSTRACT

When spacecraft dynamics are described by a Linear Fractional Representation (LFR)—as is standard in robust AOCS design—analysing the estimation and control loops in isolation no longer reflects true closed-loop behaviour, because parametric uncertainties cause attitude and orbit determination errors to become intrinsically coupled with the control law. This paper addresses that gap by introducing a unified family of sensitivity functions that captures the coupled dynamics of attitude estimation and control actuation. Building on these joint sensitivity functions, a systematic framework for in-orbit system identification of the LFR has been developed. Multisine excitation signals are tuned by optimising the spectral properties of the Fisher Information Matrix (FIM), constructed directly from sensitivity gradients derived from the system LFR. An optimal experiment design is obtained by exciting the five structurally distinct injection points available in the AOCS architecture. Together, these results enable rigorous, frequency-domain verification of stability margins, knowledge error budgets, and pointing error budgets directly from flight data.

Keywords: Pointing, Robust Control, Robust Navigation, AOCS, LFT, System Identification, Fisher Information

Nomenclature

Plant and Uncertainty

$\mathcal{P}$	=	satellite linearised dynamics model
$\mathcal{M}_{\mathcal{P}}$	=	nominal part of the LFR satellite model
$\Delta_{\mathcal{P}}$	=	uncertainty block of the LFR satellite model
$\{\delta_k\}$	=	set of scalar uncertain parameters in $\Delta_{\mathcal{P}}$
n_d	=	number of scalar uncertain parameters

Controller and Navigation

$\mathcal{N}$	=	navigation filter transfer matrix
$\mathcal{K}$	=	control law transfer matrix

System Signals

$u \in \mathbb{R}^m$	=	total torques and forces applied to satellite
$u_o \in \mathbb{R}^m$	=	commanded control torques and forces
$d_i \in \mathbb{R}^m$	=	external disturbance torques and forces
$w \in \mathbb{R}^q$	=	process disturbance
$y \in \mathbb{R}^p$	=	sensed output (measured state)

$y_n \in \mathbb{R}^p$ = noise-corrupted sensed output
$n \in \mathbb{R}^p$ = knowledge error sources (sensor noise)
$z \in \mathbb{R}^n$ = true satellite state
$\hat{y} \in \mathbb{R}^p$ = filtered sensed output (navigation estimate of y)
$\hat{z} \in \mathbb{R}^n$ = estimated satellite state
$r \in \mathbb{R}^n$ = guidance reference profile
$i \in \mathbb{R}^p$ = filter innovation signal
$\tilde{e} \in \mathbb{R}^n$ = control error ($r - \hat{z}$)
$e \in \mathbb{R}^n$ = pointing error ($r - z$)
$\tilde{z} \in \mathbb{R}^n$ = knowledge error ($z - \hat{z}$)

Sensitivity Functions and Loop Gains

$\hat{\mathcal{P}}_y$ = output system estimate
$\hat{\mathcal{P}}_z$ = state system estimate
$\hat{\mathcal{L}}_i$ = input loop gain estimate
$\hat{\mathcal{L}}_o$ = output loop gain estimate
$\hat{\mathcal{S}}_i, \hat{\mathcal{S}}_o$ = input/output sensitivity function estimates
$\hat{\mathcal{T}}_i, \hat{\mathcal{T}}_o$ = input/output complementary sensitivity function estimates
$\mathcal{S}_i, \mathcal{S}_o$ = unbiased input/output sensitivity functions
$\mathcal{T}_i, \mathcal{T}_o$ = unbiased input/output complementary sensitivity functions
P^y = output-filtering sensitivity of the navigation filter
M^y = complementary output-filtering sensitivity ($I_p - P^y = \mathcal{N}_{\hat{y}y_n}$)

Alignment Errors

$F_o \in \mathbb{C}^{p\times p}$ = output complex gain gauge
$F_i \in \mathbb{C}^{m\times m}$ = input complex gain gauge
θ_e = sensor-to-payload misalignment angle vector
θ_c = actuator assembly error angle vector

System Identification

$r_c \in \mathbb{R}^{n_c}$ = injected calibration signal
n_c = number of calibration input channels
n_y = number of identification output channels
N_c = number of excited frequencies (excitation order)
ω_k = k-th excitation frequency
$\Delta\omega$ = frequency resolution
T_{meas} = measurement window duration
$A_{j,k}$ = amplitude of channel j at frequency ω_k
$\phi_{j,k}$ = phase of channel j at frequency ω_k
$\mathbf{a}_k \in \mathbb{C}^{n_c}$ = complex amplitude vector at frequency ω_k
$\mathcal{F}$ = identification sensitivity function (LFR)
$y_{\mathcal{F}}$ = composite identification output vector
$\mathcal{D}_{\mathcal{F}_i}(\omega)$ = LFR sensitivity gradient of $\mathcal{F}$ w.r.t. δ_i
$\mathcal{R}_{L_{\mathcal{F}}}$, $\mathcal{R}_{R_{\mathcal{F}}}$ = left and right resolvent functions of $\mathcal{F}$
$E_{\mathcal{F}_i}$ = selection matrix $\partial\Delta_{\mathcal{F}}/\partial\delta_i$
$\mathbf{w}_{k,i} \in \mathbb{C}^{n_y}$ = projected sensitivity for parameter i at frequency ω_k
$\mathbf{W}_k \in \mathbb{C}^{n_y\times n_d}$ = matrix of projected sensitivities at frequency ω_k
$\mathcal{I}(\boldsymbol{\delta})$ = Fisher Information Matrix
$C_k^{(X)}$ = output noise covariance at frequency ω_k
$\mathbf{\Phi}_{r_c}(\omega)$ = spectral density matrix of calibration signal

Disturbance Characterisation and Validation

$\xi \in \mathbb{R}^p$	=	composite measurement disturbance ($n + \mathcal{P}_{yu}\, d_i + \mathcal{P}_{yw}\, w$)
$\Xi(\omega)$	=	DFT of the composite disturbance estimate $\hat{\xi}$
$\boldsymbol{v}$	=	stacked disturbance vector $[n^T \;\; d_i^T \;\; w^T]^T$
$\boldsymbol{\Gamma}_\xi$	=	disturbance mixing matrix $[I_p \;\; \mathcal{P}_{yu} \;\; \mathcal{P}_{yw}]$
$\boldsymbol{\Phi}_n$, $\boldsymbol{\Phi}_{d_i}$, $\boldsymbol{\Phi}_w$	=	prior power spectral density matrices of n, d_i, w
$\boldsymbol{\Phi}_\xi$	=	composite disturbance PSD
$\boldsymbol{\Phi}_v$	=	block-diagonal prior PSD of $\boldsymbol{v}$

Maximum Likelihood Estimation

$\hat{\boldsymbol{\delta}}$	=	estimated parameter vector
$\boldsymbol{\delta}$	=	true parameter vector
$\rho_k(\hat{\boldsymbol{\delta}})$	=	estimation residual at frequency ω_k
$\Lambda(\hat{\boldsymbol{\delta}})$	=	log-likelihood cost function

General Notation

$\bar{\sigma}(\cdot)$	=	maximum singular value
$(\cdot)^H$	=	conjugate transpose
$(\cdot)^\dagger$	=	Moore–Penrose pseudoinverse
$(\cdot)^\times$	=	skew-symmetric (cross-product) matrix associated with a vector
$\doteq$	=	first-order approximation
$\star$	=	Redheffer star product

1 Introduction

Sensitivity functions have long provided fundamental insights into the limitations in control design [1, 2]. Analogous results exist in filtering theory, where unstable poles, non-minimum-phase zeros, and delays constrain observability in much the same way they constrain controllability [3–5]. This duality is well established, yet the two domains are rarely analysed together. The only formal attempt known to the Author is the work of Carrasco et al.[6], which assumes *unbiased* estimation (*dynamic* or *matched* filtering)—an assumption incompatible with the architecture prevalent in attitude and orbit control systems (AOCS).

Indeed, the dominant flight-proven approach to satellite attitude determination is the Multiplicative Extended Kalman Filter (MEKF), described by Markley as "the workhorse of satellite attitude determination" [7]. The standard formulation employs a six-state error model—three attitude-error components and three gyroscope bias components—and propagates the reference quaternion using bias-corrected gyroscope measurements through the kinematic equation, rather than using Euler's rotational equations driven by commanded torques [8, 9]. This technique, termed *dynamic model replacement* in the literature (or *biased*[5] or *kinematic* filtering)[10], is a deliberate design choice: incorporating a dynamics model would require accurate knowledge of the spacecraft inertia matrix, actuator calibration, thruster alignment, and disturbance torque characteristics—all quantities that are uncertain in practice [11]:"even a detailed dynamics model, such as Euler's rotational equations, will have inherent errors" [10].

In this architecture, unmodelled torques are absorbed through two channels. First, the process noise covariance is tuned to reflect expected disturbance torque levels, so that any angular rate perturbation caused by an unmodelled torque manifests as an apparent discrepancy between the gyro-propagated attitude and the sensor-measured attitude, which the filter interprets as errors and corrects accordingly. Second, slowly varying or quasi-constant unmodelled torques produce a persistent angular acceleration that appears as a systematic rate error indistinguishable from the gyroscope bias drift; the bias state absorbs this effect. The result is a filter that trades estimation optimality—in the sense of discarding information that could theoretically improve accuracy—for robustness to model uncertainty. Indeed,

comparative studies have confirmed that a dynamics-augmented filter can outperform the kinematics-only MEKF when the inertia is well known, but degrades below it once inertia uncertainty exceeds a threshold [12, 13]. Incorporating the dynamics may nonetheless provide benefits when a lower-grade gyroscope is used, on condition that the disturbance torques can be estimated and accounted for.

It is important to distinguish between two uses of the term 'separation' in AOCS practice. The separation theorem, strictly speaking, asserts that the optimal observer-based controller for a known linear plant decomposes into an independent estimator and state-feedback law. This structural property holds for any fixed realisation of the uncertain parameters. Moreover, it has been shown[14] that a separation principle extends to LFR systems: the output-feedback stabilisation problem decomposes into independent state-feedback and output-injection sub-problems, and the resulting observer-based controller retains a separation structure. However, as already noted, the separation argument "*cannot be naively carried out for the performance synthesis problem*". What does not carry over to the uncertain case is the common engineering practice of analysing and verifying the estimation and control *performance* loops independently—evaluating stability margins on the control loop alone (with the filter treated as part of the sensor suite) and evaluating knowledge error budgets on the navigation loop alone (without regard to the control law).

The present paper shows that, when these *uncertainties* are properly accounted for, navigation and control errors cannot be characterised in isolation. Both are governed by *combined sensitivity functions* that capture the closed-loop interaction between estimator and controller. A direct consequence is that the pointing error—the quantity of ultimate interest—depends on these combined sensitivities in ways that neither a pure control analysis nor a pure estimation analysis reveals. The framework thus bridges the gap between time-domain Monte Carlo simulations, which capture the interactions but offer limited design insight, and frequency-domain methods, which provide systematic design tools but are commonly applied to each loop separately.

These observations are relevant to current industry practice. The European Space Agency's Pointing Error Engineering Tool (PEET) offers a structured method for allocating pointing-error budgets between estimation and control channels [15, 16]. The Pointing Error Library (PELIB), an extension of the Satellite Dynamics Toolbox developed by DYCSYT, adds support for uncertain parameters and for the TITOP modelling formalism used with flexible multibody systems [17]. Both represent the state of the art, yet neither explicitly characterises the sensitivity functions coupling the two loops.

A natural question then arises: can the combined sensitivity functions derived from the design model be validated against actual in-orbit behaviour? The second contribution of this paper addresses this question by developing a systematic framework for in-orbit system identification of the LFR directly from closed-loop flight data. The key observation is that all unknown disturbance sources—sensor noise, external torques, and process disturbances—enter the measurable outputs through a single composite quantity, whose spectral characterisation determines the error sources during calibration. By exploiting the LFR of the sensitivity functions, the Fisher Information Matrix (FIM) for the uncertain parameters $\{\delta_k\}$ is constructed in terms of the LFR of the sensitivity gradients. Optimal experiment design criteria are then derived for multisine excitation signals that maximise the parametric information content while respecting spacecraft safety constraints.

A particular feature of the proposed identification framework is the systematic analysis of excitation signal injection points. The AOCS closed-loop architecture offers eight candidate locations for injecting a calibration signal; an exhaustive analysis of their respective sensitivity functions reveals that five are structurally independent, each exciting qualitatively distinct combinations of joint navigation-and-control sensitivities. The complementarity between these injection points ensures that the resulting FIM is well conditioned across the parameter space.

Once the uncertain parameters have been identified with quantified confidence intervals, the framework is completed by a validation pipeline that reconstructs the true in-orbit pointing and knowledge

errors from operational telemetry. A frequency-domain Wiener filter, informed by the identified plant model and prior spectral envelopes, separates the individual disturbance contributions from the composite measurement. The reconstructed errors are decomposed per source using the joint sensitivity functions, enabling a line-by-line comparison against the pointing-error budget tree. Worst-case bounds over the residual parametric uncertainty can be obtained via μ-analysis, and an iterative refinement procedure progressively improves both the parametric estimates and the disturbance characterisation.

The analysis uses linearised dynamics. This is consistent with standard verification practice: although operational AOCS implementations employ nonlinear filters such as the Extended or Unscented Kalman Filter, the underlying design and verification models reduce, near the operating point, to the linear Kalman filter. Results obtained for the linearised system therefore transfer to the nonlinear setting in the small-angle regime and post-convergence steady state; large-angle slew transients, gimbal-lock neighbourhoods, and the nonlinear quaternion kinematics that motivate the MEKF's multiplicative error parameterisation lie outside the scope of this linear analysis.

This paper is organised as follows. Section 2 defines the closed-loop architecture and introduces the LFR plant model. Sections 3 and 4 derive the joint sensitivity functions for the general (biased) and matched (unbiased) cases, respectively. Section 5 discusses alignment errors, stability margins, and the Bode integral limitation. Section 6 develops the system identification framework, including the FIM construction, optimal experiment design, and injection-point analysis. Section 7 presents the post-flight validation pipeline and the iterative refinement procedure.

2 Problem Description

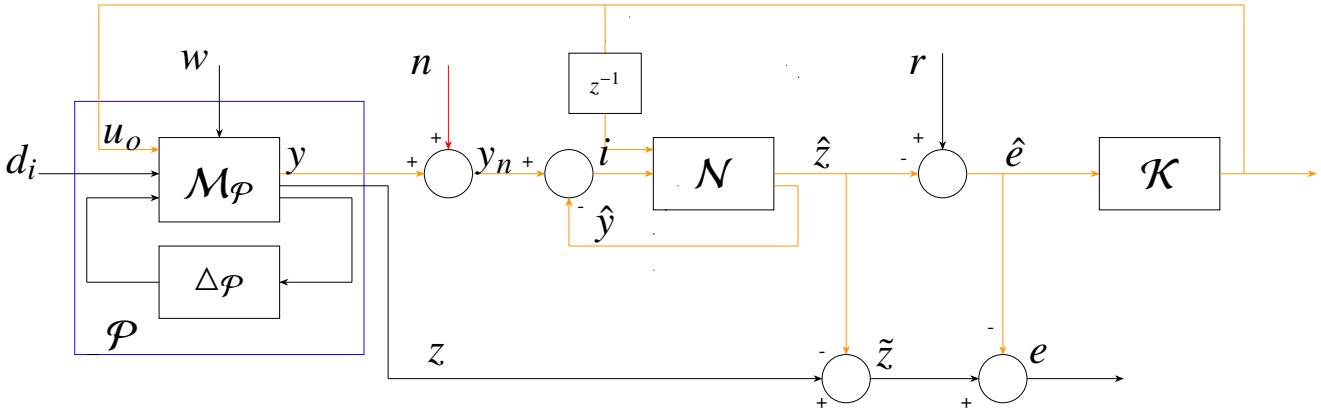

Fig. 1 AOCS closed-loop architecture: the LFR plant $\mathcal{P} = \mathcal{M}_\mathcal{P} \star \Delta_\mathcal{P}$ (blue box) is driven the commanded torques and forces u_o, disturbance torques and forces d_i and process noise w. The navigation filter $\mathcal{N}$ receives the noise-corrupted measurement y_n and - if applicable - the commanded torques and forces u_o.

It is assumed, for the sake of simplicity, that the total applied torques and forces are decomposed as

$$u = u_o + d_i \tag{1}$$

where $u_o \in \mathbb{R}^m$ is the commanded torque and force and $d_i \in \mathbb{R}^m$ is the external disturbance torque and force.

The satellite dynamics can be modelled by

$$\begin{bmatrix} y \\ z \end{bmatrix} = \begin{bmatrix} \mathcal{P}_{yu} & \mathcal{P}_{yw} \\ \mathcal{P}_{zu} & \mathcal{P}_{zw} \end{bmatrix} \begin{bmatrix} u \\ w \end{bmatrix} \tag{2}$$

where $y \in \mathbb{R}^p$ is the sensed output, $z \in \mathbb{R}^n$ is the true state, $u \in \mathbb{R}^m$ is the total applied torque and force, and $w \in \mathbb{R}^q$ is the process disturbance. Modelling uncertainties are embedded in a Linear Fractional Representation (LFR):

$$\mathcal{P} = \mathcal{M}_{\mathcal{P}} \star \Delta_{\mathcal{P}} \tag{3}$$

where $\Delta_{\mathcal{P}} \in \mathbb{R}^{d \times d}$ is a diagonal matrix of uncertain elements and $\mathcal{M}_{\mathcal{P}}$ is the purely nominal linearised dynamic model. The n_d uncertain parameters are the scalar set $\{\delta_k\}$ appearing—possibly with repetitions—on the diagonal of $\Delta_{\mathcal{P}}$. With no loss of generality, we may assume that $\mathcal{M}_{\mathcal{P}}$ can be partitioned to construct an upper linear fractional representation:

$$\mathcal{P} = \mathcal{M}_{\mathcal{P}_{22}} + \mathcal{M}_{\mathcal{P}_{21}} \Delta_{\mathcal{P}} \left(I - \mathcal{M}_{\mathcal{P}_{11}} \Delta_{\mathcal{P}} \right)^{-1} \mathcal{M}_{\mathcal{P}_{12}} \tag{4}$$

The noise-corrupted measurement is

$$y_n = y + n \tag{5}$$

The navigation function $\mathcal{N}$ is partitioned as

$$\begin{bmatrix} \hat{y} \\ \hat{z} \end{bmatrix} = \begin{bmatrix} \mathcal{N}_{\hat{y}y_n} & \mathcal{N}_{\hat{y}u_o} \\ \mathcal{N}_{\hat{z}y_n} & \mathcal{N}_{\hat{z}u_o} \end{bmatrix} \begin{bmatrix} y_n \\ u_o \end{bmatrix} \tag{6}$$

where $\hat{y} \in \mathbb{R}^p$ is the filtered sensed output and $\hat{z} \in \mathbb{R}^n$ is the estimated state. To simplify the notation, the z^{-1} term is absorbed into the filter components $\mathcal{N}_{\hat{y}u_o}$ and $\mathcal{N}_{\hat{z}u_o}$. The innovation i is:

$$i = y_n - \hat{y} \tag{7}$$

Indeed, the navigation function in eq.6 is constructed from the navigation filter described in Fig.1, having as input the innovation error i and the control command u_o:

$$\begin{bmatrix} \hat{y} \\ \hat{z} \end{bmatrix} = \begin{bmatrix} \mathcal{N}^I_{\hat{y}i} & \mathcal{N}^I_{\hat{y}u_o} \\ \mathcal{N}^I_{\hat{z}i} & \mathcal{N}^I_{\hat{z}u_o} \end{bmatrix} \begin{bmatrix} i \\ u_o \end{bmatrix} \tag{8}$$

Thus, the navigation function in eq.6 can be expressed by the closed-loop realization of the filter in eq.8:

$$\begin{bmatrix} \mathcal{N}_{\hat{y}y_n} & \mathcal{N}_{\hat{y}u_o} \\ \mathcal{N}_{\hat{z}y_n} & \mathcal{N}_{\hat{z}u_o} \end{bmatrix} = \begin{bmatrix} \left(I_p + \mathcal{N}^I_{\hat{y}i} \right)^{-1} \mathcal{N}^I_{\hat{y}i} & \left(I_p + \mathcal{N}^I_{\hat{y}i} \right)^{-1} \mathcal{N}^I_{\hat{y}u_o} \\ \mathcal{N}^I_{\hat{z}i} \left(I_p + \mathcal{N}_{\hat{y}i} \right)^{-1} & \mathcal{N}^I_{\hat{z}u_o} - \mathcal{N}^I_{\hat{z}i} \left(I_p + \mathcal{N}^I_{\hat{y}i} \right)^{-1} \mathcal{N}^I_{\hat{y}u_o} \end{bmatrix} \tag{9}$$

To simplify the notation, the partition in eq.6 shall be preferred.

The knowledge error $\tilde{z}$, control error $\tilde{e}$, and pointing error e are respectively:

$$\tilde{z} = z - \hat{z}, \tag{10}$$

$$\tilde{e} = r - \hat{z}, \tag{11}$$

$$e = r - z = \tilde{e} - \tilde{z}. \tag{12}$$

The control law computes the commanded torque from the control error:

$$u_o = \mathcal{K}\tilde{e} \tag{13}$$

To introduce pointing error sensitivity analysis it is useful to define the *output system estimate*

$$\hat{\mathcal{P}}_y = \mathcal{N}_{\hat{y}u_o} + \mathcal{N}_{\hat{y}y_n} \mathcal{P}_{yu} \tag{14}$$

and the *state system estimate*

$$\hat{\mathcal{P}}_z = \mathcal{N}_{\hat{z}u_o} + \mathcal{N}_{\hat{z}y_n}\mathcal{P}_{yu}. \tag{15}$$

With these, the *estimated loop gains* may also be defined:

$$\hat{\mathcal{L}}_i = \mathcal{K}\hat{\mathcal{P}}_z, \tag{16}$$

$$\hat{\mathcal{L}}_o = \hat{\mathcal{P}}_z\mathcal{K}. \tag{17}$$

The corresponding *return-difference matrices* yield the estimated sensitivity functions [18]:

$$\hat{\mathcal{S}}_i = \left(I_m + \hat{\mathcal{L}}_i\right)^{-1}, \tag{18}$$

$$\hat{\mathcal{S}}_o = \left(I_n + \hat{\mathcal{L}}_o\right)^{-1}, \tag{19}$$

$$\hat{\mathcal{T}}_i = \hat{\mathcal{L}}_i\left(I_m + \hat{\mathcal{L}}_i\right)^{-1}, \tag{20}$$

$$\hat{\mathcal{T}}_o = \hat{\mathcal{L}}_o\left(I_n + \hat{\mathcal{L}}_o\right)^{-1}. \tag{21}$$

The following identities hold by construction:

$$\hat{\mathcal{S}}_i + \hat{\mathcal{T}}_i = I_m, \tag{22}$$

$$\hat{\mathcal{S}}_o + \hat{\mathcal{T}}_o = I_n, \tag{23}$$

$$\mathcal{K}\hat{\mathcal{S}}_o = \hat{\mathcal{S}}_i\mathcal{K}. \tag{24}$$

3 Biased Sensitivity Analysis

In this Section, we consider $\mathcal{N}$ in full generality, encompassing even the standard kinematic filter, which does not incorporate the commanded input u_o in its design, by setting $\mathcal{N}_{\hat{z}u_o}$ and $\mathcal{N}_{\hat{y}u_o}$ to zero. The closed-loop dynamics of each system signal are derived by algebraic manipulation of the equations in Section 2.

The commanded torque is

$$u_o = \hat{\mathcal{S}}_i\mathcal{K}r - \hat{\mathcal{S}}_i\mathcal{K}\mathcal{N}_{\hat{z}y_n}n - \hat{\mathcal{S}}_i\mathcal{K}\mathcal{N}_{\hat{z}y_n}\mathcal{P}_{yu}d_i - \hat{\mathcal{S}}_i\mathcal{K}\mathcal{N}_{\hat{z}y_n}\mathcal{P}_{yw}w. \tag{25}$$

The total torque and forces are:

$$u = \hat{\mathcal{S}}_i\mathcal{K}r - \hat{\mathcal{S}}_i\mathcal{K}\mathcal{N}_{\hat{z}y_n}n + \left(I_m - \hat{\mathcal{S}}_i\mathcal{K}\mathcal{N}_{\hat{z}y_n}\mathcal{P}_{yu}\right)d_i - \hat{\mathcal{S}}_i\mathcal{K}\mathcal{N}_{\hat{z}y_n}\mathcal{P}_{yw}w. \tag{26}$$

The control error is:

$$\tilde{e} = \hat{\mathcal{S}}_o r - \hat{\mathcal{S}}_o\mathcal{N}_{\hat{z}y_n}n - \hat{\mathcal{S}}_o\mathcal{N}_{\hat{z}y_n}\mathcal{P}_{yu}d_i - \hat{\mathcal{S}}_o\mathcal{N}_{\hat{z}y_n}\mathcal{P}_{yw}w. \tag{27}$$

The sensed state is:

$$y = \mathcal{P}_{yu}\hat{\mathcal{S}}_i\mathcal{K}r - \mathcal{P}_{yu}\hat{\mathcal{S}}_i\mathcal{K}\mathcal{N}_{\hat{z}y_n}n + \mathcal{P}_{yu}\left(I_m - \hat{\mathcal{S}}_i\mathcal{K}\mathcal{N}_{\hat{z}y_n}\mathcal{P}_{yu}\right)d_i + \left(I_p - \mathcal{P}_{yu}\hat{\mathcal{S}}_i\mathcal{K}\mathcal{N}_{\hat{z}y_n}\right)\mathcal{P}_{yw}w. \tag{28}$$

The measured state is:

$$y_n = \mathcal{P}_{yu}\hat{\mathcal{S}}_i\mathcal{K}r + \left(I_p - \mathcal{P}_{yu}\hat{\mathcal{S}}_i\mathcal{K}\mathcal{N}_{\hat{z}y_n}\right)n + \mathcal{P}_{yu}\left(I_m - \hat{\mathcal{S}}_i\mathcal{K}\mathcal{N}_{\hat{z}y_n}\mathcal{P}_{yu}\right)d_i + \left(I_p - \mathcal{P}_{yu}\hat{\mathcal{S}}_i\mathcal{K}\mathcal{N}_{\hat{z}y_n}\right)\mathcal{P}_{yw}w. \tag{29}$$

The true state is:

$$z = \mathcal{P}_{zu}\hat{\mathcal{S}}_i\mathcal{K}r - \mathcal{P}_{zu}\hat{\mathcal{S}}_i\mathcal{K}\mathcal{N}_{\hat{z}y_n}n + \mathcal{P}_{zu}\left(I_m - \hat{\mathcal{S}}_i\mathcal{K}\mathcal{N}_{\hat{z}y_n}\mathcal{P}_{yu}\right)d_i + \left(\mathcal{P}_{zw} - \mathcal{P}_{zu}\hat{\mathcal{S}}_i\mathcal{K}\mathcal{N}_{\hat{z}y_n}\mathcal{P}_{yw}\right)w. \tag{30}$$

It is paramount to highlight the substantial distinction between sensitivities to d_i and w. The former pertains to a direct control sensitivity, whereas the latter constitutes an *indirect* control problem [19, 20]. The state estimate is:

$$\hat{z} = \hat{\mathcal{T}}_o r + \hat{\mathcal{S}}_o\mathcal{N}_{\hat{z}y_n}\left(n + \mathcal{P}_{yu}d_i + \mathcal{P}_{yw}w\right). \tag{31}$$

The filtered sensed output is:

$$\hat{y} = \hat{\mathcal{P}}_y\hat{\mathcal{S}}_i\mathcal{K}r + \left(\mathcal{N}_{\hat{y}y_n} - \hat{\mathcal{P}}_y\hat{\mathcal{S}}_i\mathcal{K}\mathcal{N}_{\hat{z}y_n}\right)\left(n + \mathcal{P}_{yu}d_i + \mathcal{P}_{yw}w\right). \tag{32}$$

The innovation is:

$$i = \left(\mathcal{P}_{yu} - \hat{\mathcal{P}}_y\right)\hat{\mathcal{S}}_i\mathcal{K}r + \left(I_p - \mathcal{N}_{\hat{y}y_n} - \left(\mathcal{P}_{yu} - \hat{\mathcal{P}}_y\right)\hat{\mathcal{S}}_i\mathcal{K}\mathcal{N}_{\hat{z}y_n}\right)\left(n + \mathcal{P}_{yu}d_i + \mathcal{P}_{yw}w\right). \tag{33}$$

The knowledge error is:

$$\begin{aligned}\tilde{z} = &\left(\mathcal{P}_{zu} - \hat{\mathcal{P}}_z\right)\hat{\mathcal{S}}_i\mathcal{K}r - \left(I_n + \left(\mathcal{P}_{zu} - \hat{\mathcal{P}}_z\right)\hat{\mathcal{S}}_i\mathcal{K}\right)\mathcal{N}_{\hat{z}y_n}n \\ &+ \left(\mathcal{P}_{zu} - \mathcal{N}_{\hat{z}y_n}\mathcal{P}_{yu} - \left(\mathcal{P}_{zu} - \hat{\mathcal{P}}_z\right)\hat{\mathcal{S}}_i\mathcal{K}\mathcal{N}_{\hat{z}y_n}\mathcal{P}_{yu}\right)d_i \\ &+ \left(\mathcal{P}_{zw} - \mathcal{N}_{\hat{z}y_n}\mathcal{P}_{yw} - \left(\mathcal{P}_{zu} - \hat{\mathcal{P}}_z\right)\hat{\mathcal{S}}_i\mathcal{K}\mathcal{N}_{\hat{z}y_n}\mathcal{P}_{yw}\right)w.\end{aligned} \tag{34}$$

Finally, the pointing error is:

$$\begin{aligned}e = &\left(\hat{\mathcal{S}}_o - \left(\mathcal{P}_{zu} - \hat{\mathcal{P}}_z\right)\hat{\mathcal{S}}_i\mathcal{K}\right)r \\ &+ \left(\hat{\mathcal{T}}_o + \left(\mathcal{P}_{zu} - \hat{\mathcal{P}}_z\right)\hat{\mathcal{S}}_i\mathcal{K}\right)\mathcal{N}_{\hat{z}y_n}n \\ &+ \left(-\mathcal{P}_{zu} + \left(\hat{\mathcal{T}}_o + \left(\mathcal{P}_{zu} - \hat{\mathcal{P}}_z\right)\hat{\mathcal{S}}_i\mathcal{K}\right)\mathcal{N}_{\hat{z}y_n}\mathcal{P}_{yu}\right)d_i \\ &+ \left(-\mathcal{P}_{zw} + \left(\hat{\mathcal{T}}_o + \left(\mathcal{P}_{zu} - \hat{\mathcal{P}}_z\right)\hat{\mathcal{S}}_i\mathcal{K}\right)\mathcal{N}_{\hat{z}y_n}\mathcal{P}_{yw}\right)w.\end{aligned} \tag{35}$$

4 Unbiased Sensitivity Analysis

In this Section, we assume that dynamics are embedded in the design of the filter and therefore the commanded torques and forces u_o are exploited in the filter design, making the navigation function a *dynamic filter*.

By analysing eq.14 and eq.15, the following *control matching* (or unbiasing) conditions can be set as design objectives over a meaningful frequency band:

$$\mathcal{N}_{\hat{z}u_o} \approx \mathcal{P}_{zu} - \mathcal{N}_{\hat{z}y_n}\mathcal{P}_{yu}, \tag{36}$$

$$\mathcal{N}_{\hat{y}u_o} \approx \mathcal{P}_{yu} - \mathcal{N}_{\hat{y}y_n}\mathcal{P}_{yu}. \tag{37}$$

It should be noted that these conditions can only be satisfied approximately for two reasons. First, the filter must attenuate noise n at high frequencies, which necessarily creates a mismatch in that region. Second, the uncertainty term $\Delta_{\mathcal{P}}$ in eq.3 introduces unknown dynamic feedback that prevents exact matching.

The matching conditions are therefore useful for the nominal system tuning (assuming that $\Delta_{\mathcal{P}} \ll I_d$), but must not be used for verification.

Under the simplification of eqs.36–37, the following approximate equalities hold: $\mathcal{P}_{zu} \approx \hat{\mathcal{P}}_z$, $\mathcal{P}_{yu} \approx \hat{\mathcal{P}}_y$, and hence $\hat{\mathcal{S}}_i \approx \mathcal{S}_i$, $\hat{\mathcal{T}}_i \approx \mathcal{T}_i$, $\hat{\mathcal{S}}_o \approx \mathcal{S}_o$, $\hat{\mathcal{T}}_o \approx \mathcal{T}_o$, recovering the classical MIMO control sensitivities. The unbiased closed-loop equations simplify to:

$$u_o \approx \mathcal{S}_i\mathcal{K}r - \mathcal{S}_i\mathcal{K}\mathcal{N}_{\hat{z}y_n}\left(n + \mathcal{P}_{yu}d_i + \mathcal{P}_{yw}w\right) \tag{38}$$

$$u \approx \mathcal{S}_i\mathcal{K}r - \mathcal{S}_i\mathcal{K}\mathcal{N}_{\hat{z}y_n}n - \left(I_m - \mathcal{S}_i\mathcal{K}\mathcal{N}_{\hat{z}y_n}\mathcal{P}_{yu}\right)d_i - \mathcal{S}_i\mathcal{K}\mathcal{N}_{\hat{z}y_n}\mathcal{P}_{yw}w \tag{39}$$

$$\tilde{e} \approx \mathcal{S}_o r - \mathcal{S}_o\mathcal{N}_{\hat{z}y_n}n - \mathcal{S}_o\mathcal{N}_{\hat{z}y_n}\mathcal{P}_{yu}d_i - \mathcal{S}_o\mathcal{N}_{\hat{z}y_n}\mathcal{P}_{yw}w \tag{40}$$

$$y = \mathcal{P}_{yu}\mathcal{S}_i\mathcal{K}r - \mathcal{P}_{yu}\mathcal{S}_i\mathcal{K}\mathcal{N}_{\hat{z}y_n}n + \mathcal{P}_{yu}\left(I_m - \mathcal{S}_i\mathcal{K}\mathcal{N}_{\hat{z}y_n}\mathcal{P}_{yu}\right)d_i + \left(I_p - \mathcal{P}_{yu}\mathcal{S}_i\mathcal{K}\mathcal{N}_{\hat{z}y_n}\right)\mathcal{P}_{yw}w \tag{41}$$

$$y_n \approx \mathcal{P}_{yu}\mathcal{S}_i\mathcal{K}r + \left(I_p - \mathcal{P}_{yu}\mathcal{S}_i\mathcal{K}\mathcal{N}_{\hat{z}y_n}\right)n + \mathcal{P}_{yu}\left(I_m - \mathcal{S}_i\mathcal{K}\mathcal{N}_{\hat{z}y_n}\mathcal{P}_{yu}\right)d_i + \left(I_p - \mathcal{P}_{yu}\mathcal{S}_i\mathcal{K}\mathcal{N}_{\hat{z}y_n}\right)\mathcal{P}_{yw}w \tag{42}$$

$$z \approx \mathcal{T}_o r - \mathcal{T}_o\mathcal{N}_{\hat{z}y_n}n + \mathcal{P}_{zu}\left(I_m - \mathcal{S}_i\mathcal{K}\mathcal{N}_{\hat{z}y_n}\mathcal{P}_{yu}\right)d_i + \left(\mathcal{P}_{zw} - \mathcal{P}_{zu}\mathcal{S}_i\mathcal{K}\mathcal{N}_{\hat{z}y_n}\mathcal{P}_{yw}\right)w \tag{43}$$

$$\hat{z} \approx \mathcal{T}_o r + \mathcal{S}_o\mathcal{N}_{\hat{z}y_n}\left(n + \mathcal{P}_{yu}d_i + \mathcal{P}_{yw}w\right) \tag{44}$$

$$\hat{y} \approx \mathcal{T}_o r + \left(\mathcal{N}_{\hat{y}y_n} - \mathcal{P}_{yu}\mathcal{S}_i\mathcal{K}\mathcal{N}_{\hat{z}y_n}\right)\left(n + \mathcal{P}_{yu}d_i + \mathcal{P}_{yw}w\right) \tag{45}$$

$$\tilde{z} \approx -\mathcal{N}_{\hat{z}y_n}n + \left(\mathcal{P}_{zu} - \mathcal{N}_{\hat{z}y_n}\mathcal{P}_{yu}\right)d_i + \left(\mathcal{P}_{zw} - \mathcal{N}_{\hat{z}y_n}\mathcal{P}_{yw}\right)w \tag{46}$$

$$i \approx \left(I_p - \mathcal{N}_{\hat{y}y_n}\right)\left(n + \mathcal{P}_{yu}d_i + \mathcal{P}_{yw}w\right) \tag{47}$$

$$e \approx \mathcal{S}_o r + \mathcal{T}_o\mathcal{N}_{\hat{z}y_n}n - \left(\mathcal{P}_{zu} - \mathcal{T}_o\mathcal{N}_{\hat{z}y_n}\mathcal{P}_{yu}\right)d_i - \left(\mathcal{P}_{zw} - \mathcal{T}_o\mathcal{N}_{\hat{z}y_n}\mathcal{P}_{yw}\right)w \tag{48}$$

Eq. 46 reveals that, under perfect matching, the knowledge error sources n are transferred only by the filter $\mathcal{N}_{\hat{z}y_n}$. This is the mechanism underlying the common practice of analysing the navigation loop in isolation—a practice that is valid in the nominal, matched case but, as shown in Section 3, ceases to hold when plant uncertainties or matching errors are present. The unbiased innovation in eq.47, shows the complementarity between knowledge-error and innovation sensitivity to n, already highlighted in [5]. If $z = y$, eq.48 is directly related to eqs.40 and 46, sharing the same sensitivity functions.

While it may seem natural to apply the sensitivity functions from the unbiased analysis, most AOCS designs employ kinematic filtering designs and are governed by the sensitivities described in Section 3.

5 Remarks

5.1 Alignment Errors

On-ground calibration residuals, launch-induced misalignments, and depressurisation effects may lead to misalignments between measured sensor frames before launch and real in-orbit sensor frames. Some practitioners model such effects as time-constant knowledge error sources [21]. In reality, misalignments of this kind act as gain perturbations on the sensed output y and therefore affect the stability margins.

This may be formalised by introducing a complex gain gauge $F_o \in \mathbb{C}^{p\times p}$ that perturbs the nominal output. A polar decomposition gives:

$$F_o = UH = ER_\theta\Lambda H \tag{49}$$

where H is a positive semi-adjoint matrix such that $H = H^* = \left(F_o^\dagger F_o\right)^{1/2}$ and $U = F_o H^{-1}$ is a unitary matrix such that $U^\dagger U = I_p$. The matrix H contains the pure "stretching" effect given by nonnominal scale factors, while matrix U contains the "phase" effect on the system. For multivariable systems, this includes both delays and rotations or reflection effects. Indeed, such effects can be isolated by

computing an eigendecomposition of $U = V\Lambda V^*$ such that $R_\theta = U\Lambda^{-1}$ and $\Lambda = diag\left(e^{i\Theta_1}, \dots e^{i\Theta_p}\right)$. The misalignment effects are all packed in R_θ. By computing R_θ, an undesired reflection may still arise and must be factored out. To this end, an additional matrix $E = diag(\det(R_\theta), 1, \dots, 1)$ is introduced to eliminate any residual reflection component. Adding a rotation R_θ to F_o evidently affects the disk of F_o values for which the closed loop is stable, namely the system *disk margin*[22].

From a performance point of view, to consider such unknown rotations as biases implies that the effect on the performance indexes is scaled by the DC gain of the sensitivity function. For instance, the effect on the unbiased knowledge error would be scaled by the DC gain of $N_{\hat{z}y_n}$ and the effect on the unbiased pointing error would be scaled by the DC gain of $\mathcal{T}_o\mathcal{N}_{\hat{z}y_n}$. In reality, this is not the case. But eq.34 allows to understand why this effect may be *perceived* as a bias on the knowledge error $\tilde{z}$. To prove this, it is sufficient to see the effect on the knowledge error if the difference between z and y is assumed to be only given by the misalignment error θ_e: $y = \left(I_p + \theta_e^\times\right) z$ and therefore $\mathcal{P}_{yu} = \left(I_p + \theta_e^\times\right) \mathcal{P}_{zu}$. Under this assumption, it can be noticed that by comparing eq.34 an additional knowledge error component linearly dependent to $\theta_e^\times$ can be seen:

$$\tilde{z}_\theta \doteq \mathcal{N}_{\hat{z}y_n}\theta_e^\times \left(-\mathcal{P}_{zu}\hat{\mathcal{S}}_i\mathcal{K}r + \mathcal{P}_{zu}\hat{\mathcal{S}}_i\mathcal{K}\mathcal{N}_{\hat{z}y_n}n - \left(I_n - \mathcal{P}_{zu}\hat{\mathcal{S}}_i\mathcal{K}\mathcal{N}_{\hat{z}y_n}\right)\mathcal{P}_{zu}d_i - \left(I_n - \mathcal{P}_{zu}\hat{\mathcal{S}}_i\mathcal{K}\mathcal{N}_{\hat{z}y_n}\right)\mathcal{P}_{zw}w\right) \tag{50}$$

Indeed, in the right hand side of eq.50 the additional sensitivities due to the guidance signal r, the knowledge error sources n, the disturbance torques and forces d_i and the process disturbance w is shown. Thus, the additional *bias* on the knowledge error is actually given by time-contant components of r, n, d_i and w. Yet, this is not the only effect on performances as the closed-loop sensitivity functions in eqs.18-21 would differ as well.

Let's analyse now the effect of actuator assembly errors θ_c: $u = \left(I_m + \theta_c^\times\right) u_o$. In the same way as for θ_e, the effect on the stability margins may be proven by introducing a complex gain gauge matrix $F_i \in \mathbf{C}^{m\times m}$ at the input.

From a performance point of view, we may consider from eq.48 analogously its additional effect on the pointing error e closed loop dynamics in eq.35:

$$e_\theta \doteq \mathcal{N}_{\hat{z}y_n}\mathcal{P}_{yu}\theta_c^\times\hat{\mathcal{S}}_i\mathcal{K}r - \mathcal{N}_{\hat{z}y_n}\mathcal{P}_{zu}\theta_c^\times\hat{\mathcal{S}}_i\mathcal{K}\mathcal{N}_{\hat{z}y_n}n - \mathcal{N}_{\hat{z}y_n}\mathcal{P}_{zu}\theta_c^\times\hat{\mathcal{S}}_i\mathcal{K}\mathcal{N}_{\hat{z}y_n}\mathcal{P}_{yu}d_i + \mathcal{P}_{zu}\theta_c^\times\hat{\mathcal{S}}_i\mathcal{K}\mathcal{N}_{\hat{z}y_n}\mathcal{P}_{yw}w \tag{51}$$

Indeed, in the right hand side of eq.51 additional sensitivities due to the guidance signal r, the knowledge error sources n, the disturbance torques and forces d_i and the process disturbance w is shown. An additional *bias* on the pointing error is thus given by the time-constant components of r, n, d_i and w. Obviously, just as for the sensor misalignments, this is not the only effect on performances as the closed loop sensitivity functions would differ as well from the nominal ones.

The effects of actuator and sensor misalignments have been shown on the pointing error and on the knowledge error respectively. Eq.50 and eq.51 are only provided as examples. All misalignments have a global effect on the system equations and introduce additional sensitivities on all the outputs in eqs.25-35. Both input and output misalignments can be represented as elements of $\{\delta_i\}$ and modelled in a LFR as in eq.3.

5.2 Stability Margins

As recalled in [21], stability margins like gain and phase margins were especially needed to be verified by the first generation control loops, as they were implemented with analogue devices, prone by nature to gain and phase shifts due to thermal and ageing effects on hardware components. Today the uncertainty given by the control loop is not as important given that digital control and navigation software are highly reliable. Nevertheless, especially in the *new space industry*, uncertainties given by

ageing effects on system hardware and also modelling uncertainties given by limited prior knowledge of the payloads characteristics, especially when defining generic controllers and navigation filters for a range of missions, can have an effect on the AOCS performances and stability.

Most commonly, the stability margin analysis is considered carried out by modelling the navigation system as an integral part of the sensor suite, namely as if it is part of the *plant*. Other times it is simply neglected as if the control stability problem and the filtering problem are not related at all since they respond to different specifications. Both practices are justified, implicitly or explicitly, by an appeal to the separation principle. As discussed in the preceding sections, the separation theorem itself remains valid for any fixed plant realisation; however, performances are not captured by unbiased sensitivity functions both because kinematic filtering is often preferred and because of non-perfect matching given by parametric dispersions. For instance, it has been shown, through the effects of sensor and actuator misalignments, that uncertainties at both the input and output breakpoints introduce a mismatch that effectively changes the system disk margin and both knowledge and pointing error budgets.

Stability margins can be characterized in the most general way according to the $\mathcal{S}$ and $\mathcal{T}$ criteria[21] by bounding the following peaks:

$$\begin{aligned} &\max_{\omega} \bar{\sigma}\left(\hat{\mathcal{T}}_i(j\omega)\right) \\ &\max_{\omega} \bar{\sigma}\left(\hat{\mathcal{S}}_i(j\omega)\right) \\ &\max_{\omega} \bar{\sigma}\left(\hat{\mathcal{T}}_o(j\omega)\right) \\ &\max_{\omega} \bar{\sigma}\left(\hat{\mathcal{S}}_o(j\omega)\right) \end{aligned} \tag{52}$$

Where it is to be emphasized that the sensitivity functions with which the stability analysis in eq.52 is described are mixed control-filtering sensitivities as described in Section 2.

5.3 Bode Integral

A revised Bode formula for MIMO system has been recently introduced[23], showing that the Bode integral can be written as a difference between the open-loop and closed-loop eigenvalues:

$$\sum_{i=1}^{p} \int_0^{\infty} \ln \sigma_i\left(\hat{\mathcal{S}}_i(j\omega)\right) d\omega = \frac{\pi}{2} \sum_{k=1}^{n} \left(|\Re\left(\lambda_k^{ol}\right)| - |\Re\left(\lambda_k^{cl}\right)| \right) = \frac{\pi}{2} \left(\sum_{k=1}^{n} \left(\lambda_k^{cl} - \lambda_k^{ol}\right) + 2 \sum_{i=1}^{N_p} \Re(p_i) \right) \tag{53}$$

where p_k is any of the N_p unstable poles of $\mathcal{P}_{yu}$.

Eq.53 shows that not only do the unstable poles introduce a design limitation that affects the trade-off[5] between the system bandwidth and the sensitivity bounds (stability margins), a further limitation is provided by the designer's ability to keep an "equilibrium" between closed loop and open loop eigenvalues.

Moreover, as the $\hat{\mathcal{S}}_i$ includes also the navigation filters, such equilibrium should be met also considering the contribution of the poles of the filter $\mathcal{N}$. Indeed, according to the mission requirements and specifics of the system, a trade-off is required between the poles of the controller and that of the observer[24] accordingly *deciding* if it is more appropriate to have a fast observer with a slow controller or the opposite.

6 Insights in LFR Identification

A particularly valuable prospect is that of *unlocking* robust design validation by estimating the true in-orbit performance of the MIMO attitude control system directly from flight data. Post-flight system identification enables the reconstruction of the closed-loop transfer matrix, from which stability margins, disturbance rejection bandwidths, and pointing error budgets can be rigorously verified against their design specifications.

A prerequisite for formulating the identification problem is to characterise the noise environment that corrupts the measurable outputs during the calibration experiment.

6.1 Disturbance Environment During Identification

During any on-orbit calibration experiment, the externally injected excitation signal r_c is superimposed on the closed-loop system that is simultaneously driven by the natural disturbances n, d_i, and w. By inspecting the closed-loop eqs.25–33, one observes that the three unknown disturbance vectors enter every measurable signal exclusively through a single composite quantity:

$$\xi \triangleq n + \mathcal{P}_{yu}\, d_i + \mathcal{P}_{yw}\, w \;\in\; \mathbb{R}^{p} \tag{54}$$

Indeed, the weights of d_i and w in each of eqs.25–33 equal those of n post-multiplied by $\mathcal{P}_{yu}$ and $\mathcal{P}_{yw}$ respectively, so that every measurable output in $y_{\mathcal{F}}$ admits the decomposition

$$y_{\mathcal{F}} = \mathcal{G}_r\, r + \mathcal{G}_\xi\, \xi, \tag{55}$$

where $\mathcal{G}_r$ and $\mathcal{G}_\xi$ collect the r- and ξ-dependent transfer functions from eqs.25, 27, 29, 31–33.

The PSD of the total disturbance is

$$\mathbf{\Phi}_\xi(\omega) = \mathbf{\Phi}_n(\omega) + \mathcal{P}_{yu}(\omega)\, \mathbf{\Phi}_{d_i}(\omega)\, \mathcal{P}_{yu}^{H}(\omega) + \mathcal{P}_{yw}(\omega)\, \mathbf{\Phi}_w(\omega)\, \mathcal{P}_{yw}^{H}(\omega), \tag{56}$$

built from the prior spectral envelopes $\mathbf{\Phi}_n$, $\mathbf{\Phi}_{d_i}$, $\mathbf{\Phi}_w$ that are the pointing error sources of the system[21].

6.2 Optimal Excitation Signal Design

Let $r_c(t) \in \mathbb{R}^{n_c}$ denote the externally injected calibration signal. A necessary condition for consistent parameter estimation is that $r_c(t)$ be *persistently exciting* of sufficiently high order. Formally, $r_c(t)$ is persistently exciting of order N_c if its power spectral density matrix $\mathbf{\Phi}_{r_c}(\omega) \in \mathbb{C}^{n_c \times n_c}$ satisfies [25]:

$$\mathbf{\Phi}_{r_c}(\omega) \succ 0 \qquad \text{for at least } N_c \text{ distinct frequencies } \omega \in [\omega_1, \omega_{N_c}], \tag{57}$$

with $\mathbf{\Phi}_{r_c}(\omega_k)$ required to be full rank at each excited frequency.

For a system parametrised by n_d unknown parameters, the minimum excitation order is $N_c \geq \lceil n_d / n_c \rceil$ [26]. The excitation signal on each input channel $j \in \{1, \ldots, n_c\}$ is constructed as a multisine:

$$r_{c_j}(t) = \sum_{k=1}^{N_c} A_{j,k} \sin\!\left(\omega_k\, t + \phi_{j,k}\right), \qquad \omega_k = \omega_1 + (k-1)\Delta\omega, \tag{58}$$

where $\Delta\omega = (\omega_{N_c} - \omega_1)/(N_c - 1)$ is the frequency resolution, inversely proportional to the measurement window $T_{\text{meas}} = 2\pi/\Delta\omega$.

Mutual orthogonality between input channels can be achieved via *interleaved frequency allocation*, where each j-th channel excites a disjoint frequency subset, guaranteeing channel decoupling at the cost of a factor-of-n_c reduction in per-channel frequency resolution.

A linear chirp traversing $[\omega_1, \omega_N]$ is generally ill-suited for MIMO identification for two reasons. First, only a single instantaneous frequency is excited at any given time, so the spectral matrix $\mathbf{\Phi}_{r_c}(\omega)$ is effectively rank-deficient over short windows, violating the persistence of excitation condition in eq.57. Second, adequate frequency-domain averaging requires a very slow sweep rate $\dot{\omega} \ll \Delta\omega^2$, demanding prohibitively long measurement windows—a critical constraint for on-orbit operations.

To efficiently design the multisine signal in eq.58, both the phases $\phi_{j,k}$ and amplitudes $A_{j,k}$ need to be optimised. The amplitudes $A_{j,k}$ are optimised by formulating an optimal experiment design problem that concentrates the excitation power in the frequency-channel combinations where the sensitivity function $\mathcal{F}$ is most sensitive to the parametric uncertainties $\{\delta_i\}$.

6.2.1 LFR sensitivities to $\{\delta_i\}$

A sensitivity function with n_y outputs and n_c inputs can be represented as an LFR (like in eq.4):

$$\mathcal{F} = M_{\mathcal{F}_{22}} + M_{\mathcal{F}_{21}} \Delta_{\mathcal{F}} \left(I - M_{\mathcal{F}_{11}} \Delta_{\mathcal{F}}\right)^{-1} M_{\mathcal{F}_{12}}. \tag{59}$$

We define the left and right *resolvent* functions as:

$$\mathcal{R}_{L_{\mathcal{F}}} \triangleq M_{\mathcal{F}_{21}} \left(I - \Delta_{\mathcal{F}} M_{\mathcal{F}_{11}}\right)^{-1}, \qquad \mathcal{R}_{R_{\mathcal{F}}} \triangleq \left(I - M_{\mathcal{F}_{11}} \Delta_{\mathcal{F}}\right)^{-1} M_{\mathcal{F}_{12}}. \tag{60}$$

The sensitivity of the LFR with respect to the scalar δ_i, accounting for its possible repetitions at diagonal positions of $\Delta_{\mathcal{F}}$, is then:

$$\mathcal{D}_{\mathcal{F}_i}(\omega) \triangleq \frac{\partial \mathcal{F}(\omega)}{\partial \delta_i} = \mathcal{R}_{L_{\mathcal{F}}}(\omega)\, E_{\mathcal{F}_i}\, \mathcal{R}_{R_{\mathcal{F}}}(\omega) \in \mathbb{C}^{n_y \times n_c}, \tag{61}$$

where $E_{\mathcal{F}_i} = \partial \Delta_{\mathcal{F}} / \partial \delta_i$ is a diagonal matrix that is 1 where the scalar δ_i is repeated in $\Delta_{\mathcal{F}}$ and 0 otherwise. See the Appendix for proof.

6.2.2 Fisher Information Matrix

Eq.61 provides the key link between the LFR uncertainty structure and the Fisher information matrix (FIM). For the multisine excitation in eq.58, the power spectral density is $\mathbf{\Phi}_{r_c}(\omega) = \frac{1}{2} \sum_{k=1}^{N_c} \mathbf{a}_k \mathbf{a}_k^H \, \delta(\omega - \omega_k)$, where $\mathbf{a}_k \in \mathbb{C}^{n_c}$ with $[\mathbf{a}_k]_j = A_{j,k} e^{i\phi_{j,k}}$.

In the presence of the coloured output noise characterised in Section 6.1, the (i, j) entry of the Fisher information matrix $\mathcal{I} \in \mathbb{C}^{n_d \times n_d}$ is [25, 27, 28]:

$$\mathcal{I}_{ij} = \frac{1}{2} \sum_{k=1}^{N_c} \mathbf{w}_{k,j}^H \left[C_k^{(X)}\right]^{-1} \mathbf{w}_{k,i}, \tag{62}$$

where $\mathbf{w}_{k,i} \triangleq \mathcal{D}_{\mathcal{F}_i}(\omega_k)\, \mathbf{a}_k \in \mathbb{C}^{n_y}$ is the *projected sensitivity* for parameter i at frequency ω_k, and $C_k^{(X)}$ is the output noise covariance:

$$C_k^{(X)} = \mathcal{G}_{\xi}^{(X)}(\omega_k)\, \mathbf{\Phi}_{\xi}(\omega_k)\, \mathcal{G}_{\xi}^{(X),H}(\omega_k) \tag{63}$$

Since $C_k^{(X)} \succ 0$ at every excited frequency, the FIM is always well defined.

Eq. 62 incorporates the *a priori* knowledge of the broadband disturbance environment. At frequencies where the broadband noise floor is low, each unit of excitation power contributes more information; conversely, a higher noise floor penalises the FIM contribution.

6.2.3 Amplitude and phase optimisation

Since in eq.62 the matrix $\mathcal{D}_{\mathcal{F}_i}(\omega_k)\,\mathbf{a}_k\mathbf{a}_k^H\,\mathcal{D}_{\mathcal{F}_j}^H(\omega_k)$ is Hermitian, and the weighting by $[C_k^{(X)}]^{-1}$ preserves this property, all spectral properties of the weighted FIM are phase independent. Consequently, the amplitudes $A_{j,k}$ can be optimized separately from the phases $\phi_{j,k}$. Indeed, provided $\mathcal{I}$ is invertible, the amplitudes $A_{j,k}$ may be optimised according to one of three classical optimality criteria [29–31]:

- *A-optimal*: min $\mathrm{tr}[\mathcal{I}^{-1}(\Delta_{\mathcal{F}})]$ — minimises total parameter variance.
- *D-optimal*: max $\log\det\mathcal{I}(\Delta_{\mathcal{F}})$ — minimises the volume of the confidence ellipsoid.
- *E-optimal*: max $\lambda_{\min}(\mathcal{I}(\Delta_{\mathcal{F}}))$ — maximises worst-case identifiability.

The amplitude design must respect safety bounds to prevent the calibration experiment from exciting the spacecraft dynamics into the nonlinear regime. Such bounds can be readily computed through standard worst-case analysis of the sensitivity function $\mathcal{F}$.

The Fisher information matrix is invertible precisely because it is a sum of Gram matrices, which in turn requires the reference signal to be a multisine. Each individual Gram matrix is rank-1; consequently, exciting the system with a single sinusoid renders the unknown parameters unidentifiable under any standard optimality criterion.

The optimization of the phases $\phi_{j,k}$ can be carried out to minimize the crest-factor of the frequency response with the use of a Chebyshev norms-based algorithm [32]. This approach enables to improve the crest-factor considerably compared to Schroeder phasing rules [33] which are optimal when the amplitudes of the multisine are kept all equal.

6.3 Maximum Likelihood Estimator

A maximum likelihood estimator of $\boldsymbol{\delta} \in \mathbb{R}^{n_d}$ can be designed to minimize the weighted estimation residual:

$$\rho_k\left(\hat{\boldsymbol{\delta}}\right) = Y_k - \mathcal{F}\left(\omega_k, \hat{\boldsymbol{\delta}}\right)\mathbf{a}_k, \tag{64}$$

where $Y_k \in \mathbb{C}^{n_y}$ denotes the measured output spectrum of $\mathcal{F}$ at frequency ω_k. The log-likelihood is defined as the weighted quadratic cost function:

$$\Lambda\left(\hat{\boldsymbol{\delta}}\right) = \sum_{k=1}^{N_c} \rho_k^H \left[C_k^{(X)}\right]^{-1} \rho_k. \tag{65}$$

Defining $\mathbf{W}_k \triangleq [\mathbf{w}_{k,1}\cdots\mathbf{w}_{k,n_d}] \in \mathbb{C}^{n_y\times n_d}$ as the matrix of projected sensitivities from eq.62, the parameters are updated iteratively via:

$$\hat{\boldsymbol{\delta}}^{(n+1)} = \hat{\boldsymbol{\delta}}^{(n)} + \frac{1}{2}\mathcal{I}^{-1}\Re\left\{\sum_{k=1}^{N_c}\mathbf{W}_k^H\left[C_k^{(X)}\right]^{-1}\rho_k\right\}, \tag{66}$$

where n denotes the iteration index. Near the true parameter values, the estimator achieves the Cramér–Rao lower bound [28]:

$$\mathrm{cov}\left(\hat{\boldsymbol{\delta}}\right) \geq \mathcal{I}^{-1}. \tag{67}$$

The incorporation of $C_k^{(X)}$ in both the cost function and the update rule ensures that the estimator is efficient: it extracts the maximum amount of information from the data given the actual noise environment, rather than treating all frequencies equally.

Given that the uncertain parameters $\{\delta_k\}$ are defined *in open intervals*, possibly normalized in the open interval $(-1\,,\,1)$ (which is always a good practice when practically working with LFRs), and that

$\mathcal{I}$ is well conditioned, since the maximum likelihood estimator is asymptotically normal, the residual uncertainty intervals are given by:

$$\delta_i \in \hat{\delta}_i \pm z_{\alpha/2}\sqrt{\left(\mathcal{I}^{-1}\right)_{ii}} \tag{68}$$

where $z_{\alpha/2}$ is the quantile of the standard normal distribution. Once the new uncertainty intervals have been obtained, the LFR may be rescaled in order that the uncertainty intervals are normalized.

6.4 Excitation Signal Injection Points

In sections 6.2 and 6.3 considerations are carried out in general terms without making assumptions on $\mathcal{F}$. In this section, we shall argue the possible choices in defining $\mathcal{F}$.

From an intuitive standpoint, increasing the number of outputs n_y, enlarges the dimension of $\mathbf{w}_{k,j}$. Consequently, the summation defining $\mathcal{I}_{ij}$ in eq.62 comprises more terms, which generally leads to a larger value of the information metric. The natural instinct of the AOCS engineer would be to inject the optimal excitation signal r_c in the guidance and consider as an output y_n. Yet, the previous arguments suggest to take all the available outputs and therefore the choice is to define the output of $\mathcal{F}$ to be:

$$y_{\mathcal{F}} = \begin{bmatrix} u_o & \tilde{e} & y_n & \hat{z} & \hat{y} & i \end{bmatrix}^T \tag{69}$$

From eq.25, eq.27, eq.29, eq.31-33 it is clear that the sensitivities are *different* and therefore each of these contributions provides an exclusive source of information that may help determine a good $\hat{\delta}$. Indeed, some sensitivities may provide a higher sensitivity to a parameter with regards to others, by combining all these different contributions, all the information is fully exploited.

Another matter is deciding where to inject the excitation signal in the loop. This could ideally be carried out on any signal available. Indeed, there are 8 different locations in in the closed loop system in Fig.1:

A) Injection at the guidance: $r \rightarrow r + r_c$
B) Injection at the plant input, while the navigation filter ignores such injection: $u \rightarrow u + r_c$
C) Injection at the controller output, while the navigation filter is informed of such injection: $u_o \rightarrow u_o + r_c$
D) Injection at the measured state: $y_n \rightarrow y_n + r_c$
E) Injection at the filtered state output: $\hat{z} \rightarrow \hat{z} + r_c$
F) Injection at the filtered sensed output: $\hat{y} \rightarrow \hat{y} + r_c$
G) Injection at the control command at the navigation filter only (when applicable)
H) Injection at the innovation $i \rightarrow i + r_c$

6.4.1 Injection at the guidance

This is the most intuitive injection point. In practice, this injection may be interpreted as a redefinition of the guidance signal r thereby all the sensitivities in Section 3 hold:

$$y_{\mathcal{F}}^{(A)} = \mathcal{F}^{(A)} r_c^{(A)} = \begin{bmatrix} \hat{\mathcal{S}}_i\mathcal{K} \\ \hat{\mathcal{S}}_o \\ \mathcal{P}_{yu}\hat{\mathcal{S}}_i\mathcal{K} \\ \hat{\mathcal{T}}_o \\ \hat{\mathcal{P}}_y\hat{\mathcal{S}}_i\mathcal{K} \\ \left(\mathcal{P}_{yu} - \hat{\mathcal{P}}_y\right)\hat{\mathcal{S}}_i\mathcal{K} \end{bmatrix} r_c^{(A)} \tag{70}$$

What must be highlighted is that the joint navigation and control sensitivities are expected to be very much *different* in their frequency response. For instance, the sensitivities to the control error $\tilde{e}$ and the state estimate $\hat{z}$ are complementary: implying that for sure the injection signal can be made with a small amplitude $A_{j,k}$ knowing that in certain frequency ranges one of two output signals shall be excited enough to return enough information to identify the $\Delta_{\mathcal{F}}$.

6.4.2 Injection at the plant input

In this case, the injection is carried out directly at the plant input, but is ignored by the navigation system (if applicable). Effectively, this is equivalent to adding a term to the disturbance d_i described in Section 3:

$$y_{\mathcal{F}}^{(B)} = \mathcal{F}^{(B)} r_c^{(B)} = \begin{bmatrix} -\hat{\mathcal{S}}_i \mathcal{K} \mathcal{N}_{\hat{z}y_n} \mathcal{P}_{yu} \\ -\hat{\mathcal{S}}_o \mathcal{N}_{\hat{z}y_n} \mathcal{P}_{yu} \\ \mathcal{P}_{yu} \left(I_m - \hat{\mathcal{S}}_i \mathcal{K} \mathcal{N}_{\hat{z}y_n} \mathcal{P}_{yu} \right) \\ \hat{\mathcal{S}}_o \mathcal{N}_{\hat{z}y_n} \mathcal{P}_{yu} \\ \left(\mathcal{N}_{\hat{y}y_n} - \hat{\mathcal{P}}_y \hat{\mathcal{S}}_i \mathcal{K} \mathcal{N}_{\hat{z}y_n} \right) \mathcal{P}_{yu} \\ \left(I_p - \mathcal{N}_{\hat{y}y_n} - \left(\mathcal{P}_{yu} - \hat{\mathcal{P}}_y \right) \hat{\mathcal{S}}_i \mathcal{K} \mathcal{N}_{\hat{z}y_n} \right) \mathcal{P}_{yu} \end{bmatrix} r_c^{(B)} \tag{71}$$

As seen in eq.71, the two output signals $\tilde{e}$ and $\hat{z}$ are redundant. This would be a problem if the injection is performed at the plant input only: in such case, one of two outputs can be dropped as it does not provide any additional information. Otherwise, the sensitivities in eq. 71 also differ significantly in their frequency responses. In particular, $\mathcal{N}_{\hat{y}y_n}$ and $I_p - \mathcal{N}_{\hat{y}y_n}$ are complementary.

6.4.3 Injection at the controller output

In this case, the injection is carried out directly at the controller output and considered by the navigation system (if applicable). The sensitivity to such an injection signal is:

$$y_{\mathcal{F}}^{(C)} = \mathcal{F}^{(C)} r_c^{(C)} = \begin{bmatrix} \hat{\mathcal{S}}_i \\ -\hat{\mathcal{S}}_o \hat{\mathcal{P}}_z \\ \mathcal{P}_{yu} \hat{\mathcal{S}}_i \\ \hat{\mathcal{P}}_z \hat{\mathcal{S}}_i \\ \hat{\mathcal{P}}_y \hat{\mathcal{S}}_i \\ \left(\mathcal{P}_{yu} - \hat{\mathcal{P}}_y \right) \hat{\mathcal{S}}_i \end{bmatrix} r_c^{(C)} \tag{72}$$

It can be noticed that eq.72 has all non-redundant outputs and a unique opportunity to excite directly the estimated input sensitivity $\hat{\mathcal{S}}_i$.

6.4.4 Injection at the measured state

In this case, the injection is carried out at the measured plant output. In practice, this injection is equivalent to adding $r_c^{(D)}$ to the knowledge error sources n, therefore it has the same sensitivites described

in Section 3:

$$y_{\mathcal{F}}^{(D)} = \mathcal{F}^{(D)} r_c^{(D)} = \begin{bmatrix} -\hat{\mathcal{S}}_i \mathcal{K} \mathcal{N}_{\hat{z}y_n} \\ -\hat{\mathcal{S}}_o \mathcal{N}_{\hat{z}y_n} \\ I_p - \mathcal{P}_{yu} \hat{\mathcal{S}}_i \mathcal{K} \mathcal{N}_{\hat{z}y_n} \\ \hat{\mathcal{S}}_o \mathcal{N}_{\hat{z}y_n} \\ \mathcal{N}_{\hat{y}y_n} - \hat{\mathcal{P}}_y \hat{\mathcal{S}}_i \mathcal{K} \mathcal{N}_{\hat{z}y_n} \\ I_p - \mathcal{N}_{\hat{y}y_n} - \left(\mathcal{P}_{yu} - \hat{\mathcal{P}}_y\right) \hat{\mathcal{S}}_i \mathcal{K} \mathcal{N}_{\hat{z}y_n} \end{bmatrix} r_c^{(D)} \tag{73}$$

It can be noticed that in eq.73 the two output signals $\tilde{e}$ and $\hat{z}$ are redundant, in this case the same considerations mentioned in Section 6.4.2 are valid.

6.4.5 Injection at the filtered state output

If an injection is added to the filtered state output $\hat{z}$, the following sensitivity functions would be excited:

$$y_{\mathcal{F}}^{(E)} = \mathcal{F}^{(E)} r_c^{(E)} = \begin{bmatrix} -\hat{\mathcal{S}}_i \mathcal{K} \\ -\hat{\mathcal{S}}_o \\ -\mathcal{P}_{yu} \hat{\mathcal{S}}_i \mathcal{K} \\ \hat{\mathcal{S}}_o \\ -\hat{\mathcal{P}}_y \hat{\mathcal{S}}_i \mathcal{K} \\ -\left(\mathcal{P}_{yu} - \hat{\mathcal{P}}_y\right) \hat{\mathcal{S}}_i \mathcal{K} \end{bmatrix} r_c^{(E)} \tag{74}$$

Where it is to be noticed that the sensitivity functions in eq.74 eliminate those in eq.70 if these would be excited at the same frequencies. The total effect would only be a direct feedthrough of r_c on $\hat{z}$ given by the $\hat{\mathcal{T}}_o + \hat{\mathcal{S}}_o = I_n$. Thereby, as it doesn't add anything valuable the choice is not consider injecting at the filtered state output $\hat{z}$.

6.4.6 Injection at the filtered output

An injection at the filtered output $\hat{y}$ affects directly the navigation loop in eq.6:

$$\begin{bmatrix} \hat{y} \\ \hat{z} \end{bmatrix} = \begin{bmatrix} \mathcal{N}_{\hat{y}y_n} & \mathcal{N}_{\hat{y}u_o} \\ \mathcal{N}_{\hat{z}y_n} & \mathcal{N}_{\hat{z}u_o} \end{bmatrix} \begin{bmatrix} y_n \\ u_o \end{bmatrix} + \begin{bmatrix} P^y \\ -\mathcal{N}_{\hat{z}y_n} \end{bmatrix} r_c^{(F)} \tag{75}$$

What must be emphasized in eq.75 is that $r_c^{(F)}$ *excites directly* the output-filtering sensitivity P^y (see [5]): $P^y = \left(I_p + \mathcal{N}_{\hat{y}i}^I\right)^{-1}$. This sensitivity provides insight into the filtering properties of the navigation filter as P^y is the dynamic transfer between the measurement error sources n and the innovation:

$$i = P^y (y + n) - P^y \mathcal{N}_{\hat{y}u}^I u_o - P^y r_c^{(F)} \tag{76}$$

The complementary output-filtering sensitivity $M^y = I_p - P^y$ is indeed the sensitivity of the filtered output $\hat{y}$ to the measurement error sources n: $M^y = \left(I_p + \mathcal{N}_{\hat{y}i}^I\right)^{-1} \mathcal{N}_{\hat{y}i}^I = \mathcal{N}_{\hat{y}y_n}$. By construction such sensitivities are similar to the control sensitivities. It can be noticed that $\mathcal{P}^y$ is also the *unbiased* sensitivity of the innovation i to n as shown in eq.47.

In closed loop, the following sensitivities would be excited:

$$y_{\mathcal{F}}^{(F)} = \mathcal{F}^{(F)} r_c^{(F)} = \begin{bmatrix} \hat{\mathcal{S}}_i \mathcal{K} \mathcal{N}_{\hat{z} y_n} \\ \hat{\mathcal{S}}_o \mathcal{N}_{\hat{z} y_n} \\ \mathcal{P}_{yu} \hat{\mathcal{S}}_i \mathcal{K} \mathcal{N}_{\hat{z} y_n} \\ -\hat{\mathcal{S}}_o \mathcal{N}_{\hat{z} y_n} \\ \hat{\mathcal{P}}_y \hat{\mathcal{S}}_i \mathcal{K} \mathcal{N}_{\hat{z} y_n} + P^y \\ \left(\mathcal{P}_{yu} - \hat{\mathcal{P}}_y \right) \hat{\mathcal{S}}_i \mathcal{K} \mathcal{N}_{\hat{z} y_n} - P^y \end{bmatrix} r_c^{(F)} \tag{77}$$

Given the complementarity of M^y and P^y, it can be noticed that the sensitivities in eq.73 eliminate those in eq.77 if these would be excited at the same frequencies. The total effect would only be a direct feedthrough in y_n and $\hat{y}$. Thereby, as it doesn't add anything valuable the choice is to not consider injecting at the filtered output.

6.4.7 Injection at the control input of the navigation filter

If an injection is added to the control command only at the input of the navigation filter, the following sensitivity functions would be excited:

$$y_{\mathcal{F}}^{(G)} = \mathcal{F}^{(G)} r_c^{(G)} = \begin{bmatrix} -\hat{\mathcal{S}}_i \mathcal{K} \mathcal{N}_{\hat{z} u_o} \\ -\hat{\mathcal{S}}_o \mathcal{N}_{\hat{z} u_o} \\ -\mathcal{P}_{yu} \hat{\mathcal{S}}_i \mathcal{K} \mathcal{N}_{\hat{z} u_o} \\ \hat{\mathcal{S}}_o \mathcal{N}_{\hat{z} u_o} \\ \mathcal{N}_{\hat{y} u_o} - \hat{\mathcal{P}}_y \hat{\mathcal{S}}_i \mathcal{K} \mathcal{N}_{\hat{z} u_o} \\ -\mathcal{N}_{\hat{y} u_o} - \left(\mathcal{P}_{yu} - \hat{\mathcal{P}}_y \right) \hat{\mathcal{S}}_i \mathcal{K} \mathcal{N}_{\hat{z} u_o} \end{bmatrix} r_c^{(G)} \tag{78}$$

The sensitivity functions in eq.78 are original compared to the ones obtained in the previous injection points because they showcase the $\mathcal{N}_{\hat{y} u_o}$ and $\mathcal{N}_{\hat{z} u_o}$. Nevertheless, it is to be noticed, that the output signals $\tilde{e}$ and $\hat{z}$ are redundant.

6.4.8 Injection at the innovation

If an injection is added to the innovation the following sensitivity functions would be excited:

$$y_{\mathcal{F}}^{(H)} = \mathcal{F}^{(H)} r_c^{(H)} = \begin{bmatrix} -\hat{\mathcal{S}}_i \mathcal{K} \mathcal{N}_{\hat{z} y_n} \\ -\hat{\mathcal{S}}_o \mathcal{N}_{\hat{z} y_n} \\ -\mathcal{P}_{yu} \hat{\mathcal{S}}_i \mathcal{K} \mathcal{N}_{\hat{z} y_n} \\ \hat{\mathcal{S}}_o \mathcal{N}_{\hat{z} y_n} \\ -\hat{\mathcal{P}}_y \hat{\mathcal{S}}_i \mathcal{K} \mathcal{N}_{\hat{z} y_n} + \mathcal{N}_{\hat{y} y_n} \\ -\mathcal{N}_{\hat{y} y_n} - \left(\mathcal{P}_{yu} - \hat{\mathcal{P}}_y \right) \mathcal{K} \hat{\mathcal{S}}_o \mathcal{N}_{\hat{z} y_n} \end{bmatrix} r_c^{(H)} \tag{79}$$

It can be noticed that eq.79 excites essentially the same sensitivity functions of eq.73. Indeed, if both injections were to be carried out on the same frequencies the sensitivities would be eliminated yielding a feedthrough at the y_n and i channels. Thus, this injection doesn't add anything valuable.

6.5 Injection point selection

The sensitivity analysis carried out in Sections 6.4.1–6.4.8 reveals that the eight candidate injection points are not all independent: three of them can be discarded on structural grounds, leaving five that collectively provide the richest parametric information.

The five structurally independent injection points are therefore:

$$r_c = \begin{bmatrix} r_c^{(A)} & r_c^{(B)} & r_c^{(C)} & r_c^{(D)} & r_c^{(G)} \end{bmatrix}^T \tag{80}$$

Each contributes a qualitatively distinct family of sensitivity functions to the output $\mathcal{F}$:

$$y_{\mathcal{F}} = \begin{bmatrix} \mathcal{F}^{(A)} & \mathcal{F}^{(B)} & \mathcal{F}^{(C)} & \mathcal{F}^{(D)} & \mathcal{F}^{(G)} \end{bmatrix} r_c \tag{81}$$

Given the variety of sensitivity functions it is expected that the chances of exciting the system enough to obtain a well conditioned $\mathcal{I}$ matrix are good, especially for those parameters that are most impactful. Indeed, several structural features of eq.81 support the expectation that the resulting Fisher information matrix $\mathcal{I}$ will be well conditioned:

1) *Complementary sensitivity pairs.* Injection A excites $\hat{\mathcal{S}}_o$ and $\hat{\mathcal{T}}_o$ as separate output channels (rows 2 and 4 of eq.70). Since these are complementary ($\hat{\mathcal{S}}_o + \hat{\mathcal{T}}_o = I_n$), the excitation signal amplitude $A_{j,k}$ can be kept small while still guaranteeing that, at every frequency, at least one of the two channels produces a response of appreciable magnitude. Low-frequency content is predominantly captured by $\hat{\mathcal{T}}_o$, while high-frequency content is captured by $\hat{\mathcal{S}}_o$.
2) *Direct access to input sensitivity.* Injection C is the only point that excites the estimated input sensitivity $\hat{\mathcal{S}}_i$ directly as a stand-alone output channel (row 1 of eq.72). Moreover, all six output channels of eq.72 are structurally non-redundant, meaning that no pair of rows becomes proportional under any nominal parameter choice.
3) *Separation of plant and filter contributions* Injection B enters before the plant input (equivalent to an additive disturbance d_i) while Injection D enters at the measured state (equivalent to an additive sensor noise n). As a result, the plant transfer $\mathcal{P}_{yu}$ premultiplies the sensitivity matrix in Injection B (eq.71) but does not appear in the corresponding position of Injection D (eq.73). This frequency-dependent weighting difference ensures that the two injections provide linearly independent columns in the projected sensitivity vectors $\mathbf{w}_{k,i}$ of eq.62, even when the underlying parametric gradients have similar structure.
4) *Observability of the filter's input channel.* Injection G excites the navigation filter's control-command input $\mathcal{N}_{\hat{z}u_o}$ and $\mathcal{N}_{\hat{y}u_o}$ (see eq.78), which do not appear as weights in any other injection point. For AOCS architectures that incorporate commanded torques in the filter propagation, these terms carry information about the filter's internal model of the plant dynamics and are therefore essential for identifying parameters that affect the matching conditions of eqs.36–37.

Recalling from eq.62 that each entry of the Fisher information matrix is a sum of Gram inner products $\mathcal{I}_{ij} = \frac{1}{2}\sum_k \mathbf{w}_{k,j}^H \mathbf{w}_{k,i}$, the dimensionality of $\mathbf{w}_{k,i}$ grows with the total number of output channels n_y. The composite output vector $y_{\mathcal{F}}$ in eq.81 aggregates six output signals from each of the five injection points, providing up to 30 scalar output channels (before accounting for signal dimensions). The diversity of the sensitivity functions across these channels—spanning complementary pairs, direct and indirect control paths, and both the plant-side and filter-side of the loop—ensures that the projected sensitivity vectors $\mathbf{w}_{k,i}$ span a high-dimensional subspace of $\mathbb{C}^{n_y}$ for each excited frequency ω_k, which is the fundamental requirement for $\mathcal{I}$ to be well conditioned.

7 Towards Robust Pointing Validation

The system identification framework in Section 6 allows to reduce with an ad-hoc optimal experiment the uncertainties of the $\Delta_{\mathcal{P}}$ along with the residual confidence intervals of such parameters. Provided such experiment has been performed, an estimate of the true knowledge and pointing errors, in the operative *mission profile*, can be computed by exploiting the sensitivity functions in Section 3. Given the telemetry of the known signals in eq.69, it is now a matter of estimating the unknown inputs of the system n, d_i and w, allowing to recover an estimate of the true knowledge error $\tilde{z}$ and pointing error e from flight data.

The composite disturbance ξ defined in eq.54 is **directly computable** from telemetry:

$$\hat{\xi} = y_n - \mathcal{P}_{yu}\left(\hat{\Delta}_{\mathcal{P}}\right) u_o, \tag{82}$$

which is exact—no inversion is required—once $\mathcal{P}_{yu}$ is evaluated at the identified parameters $\hat{\Delta}_{\mathcal{P}}$.

Although the closed-loop telemetry constrains n, d_i, and w only through $\hat{\xi}$, the three disturbance classes can be separated by exploiting the identified plant model and prior spectral information from the mission environment analysis. At each frequency ω, the composite disturbance satisfies

$$\xi(\omega) = \mathbf{\Gamma}_{\xi}(\omega, \hat{\Delta}_{\mathcal{P}})\, \boldsymbol{\nu}(\omega), \tag{83}$$

where

$$\mathbf{\Gamma}_{\xi}(\omega, \hat{\Delta}_{\mathcal{P}}) = \begin{bmatrix} I_p & \mathcal{P}_{yu}(\omega, \hat{\Delta}_{\mathcal{P}}) & \mathcal{P}_{yw}(\omega, \hat{\Delta}_{\mathcal{P}}) \end{bmatrix} \in \mathbb{C}^{p\times(p+m+q)} \tag{84}$$

and $\boldsymbol{\nu} = \begin{bmatrix} n^T & d_i^T & w^T \end{bmatrix}^T \in \mathbb{R}^{p+m+q}$. Since $p < p+m+q$, eq.83 is underdetermined at each frequency. However, the three sources possess distinct and well-characterised spectral signatures:

- *Sensor noise n*: high-frequency content with PSD $\mathbf{\Phi}_n(\omega)$ provided by the sensor manufacturer. At frequencies well above the plant bandwidth, $\mathcal{P}_{yu} \to 0$ and $\mathcal{P}_{yw} \to 0$, so $\xi \approx n$.
- *External disturbance torques and forces d_i*: concentrated at orbital harmonics and at reaction-wheel spin frequencies, with PSD $\mathbf{\Phi}_{d_i}(\omega)$ derived from the mission environment model.
- *Process disturbance w*: broadband, defined to take into account any modelling errors or particular disturbances that can't be added to u_o.

Given the prior cross-spectral density matrix

$$\mathbf{\Phi}_{\nu}(\omega) = \mathrm{blkdiag}\big(\mathbf{\Phi}_n(\omega),\ \mathbf{\Phi}_{d_i}(\omega),\ \mathbf{\Phi}_w(\omega)\big) \tag{85}$$

and assuming mutual uncorrelation, the minimum-variance (Wiener) estimate of the individual disturbances at each frequency is

$$\hat{\boldsymbol{\nu}}(\omega) = \mathbf{\Phi}_{\nu}(\omega)\, \mathbf{\Gamma}_{\xi}^{H}(\omega, \hat{\Delta}_{\mathcal{P}}) \left[\mathbf{\Phi}_{\xi}(\omega)\right]^{-1} \Xi(\omega), \tag{86}$$

where $\mathbf{\Phi}_{\xi} = \mathbf{\Gamma}_{\xi}\, \mathbf{\Phi}_{\nu}\, \mathbf{\Gamma}_{\xi}^{H}$ as in eq.56 and $\Xi(\omega)$ is the DFT of $\hat{\xi}(t)$. Writing out the individual estimates:

$$\hat{n}(\omega) = \mathbf{\Phi}_n(\omega) \left[\mathbf{\Phi}_{\xi}(\omega)\right]^{-1} \Xi(\omega), \tag{87}$$

$$\hat{d}_i(\omega) = \mathbf{\Phi}_{d_i}(\omega)\, \mathcal{P}_{yu}^{H}(\omega) \left[\mathbf{\Phi}_{\xi}(\omega)\right]^{-1} \Xi(\omega), \tag{88}$$

$$\hat{w}(\omega) = \mathbf{\Phi}_w(\omega)\, \mathcal{P}_{yw}^{H}(\omega) \left[\mathbf{\Phi}_{\xi}(\omega)\right]^{-1} \Xi(\omega). \tag{89}$$

The PSD $\hat{\mathbf{\Phi}}_{\xi}(\omega)$ estimated directly from the telemetry via eq.82 can be compared with the model-predicted PSD from eq.56. Any significant discrepancy flags either an environment model error w or a residual parametric misidentification as defined in eq.68.

With the individual disturbance estimates in hand, the unmeasured closed-loop signals are reconstructed:

$$\hat{u} = u_o + \hat{d}_i \tag{90}$$

$$\hat{y}_{\text{true}} = y_n - \hat{n} = \mathcal{P}_{yu}(\hat{\Delta}_{\mathcal{P}})\hat{u} + \mathcal{P}_{yw}(\hat{\Delta}_{\mathcal{P}})\hat{w} \tag{91}$$

$$\hat{z}_{\text{true}} = \mathcal{P}_{zu}\left(\hat{\Delta}_{\mathcal{P}}\right)\hat{u} + \mathcal{P}_{zw}\left(\hat{\Delta}_{\mathcal{P}}\right)\hat{w} \tag{92}$$

$$\tilde{z}_{\text{true}} = \hat{z}_{\text{true}} - \hat{z} \tag{93}$$

$$\hat{e}_{\text{true}} = r - \hat{z}_{\text{true}} \tag{94}$$

The reconstructed errors can be decomposed per source using eqs.34–35 evaluated at $\hat{\Delta}_{\mathcal{P}}$, enabling a line-by-line comparison against the pointing-error budget tree. Worst-case bounds over the residual parametric uncertainty are obtained by evaluating the maximum over the confidence region, which is a standard μ-analysis problem since all transfer matrices are available in LFR form.

The identification–validation pipeline can be iterated to progressively improve both the parametric estimates and the disturbance characterisation. The outputs of the validation step—the reconstructed disturbances and their spectral decomposition—constitute refined prior information that can be fed back into the experiment design in Section 6.

The procedure begins with Iteration 0, in which the design-phase prior spectral envelopes $\mathbf{\Phi}_n^{(0)}$, $\mathbf{\Phi}_{d_i}^{(0)}$, $\mathbf{\Phi}_w^{(0)}$ are used to compute the output noise covariance $C_k^{(X,0)}$ via eq. (63), design the first calibration experiment, and obtain an initial parameter estimate $\hat{\boldsymbol{\delta}}^{(0)}$. At each subsequent iteration j, the previous estimate $\hat{\boldsymbol{\delta}}^{(j-1)}$ is exploited as follows. First, nominal-operations telemetry is recorded and the composite disturbance estimate $\hat{\boldsymbol{\xi}}^{(j)} = y_n - \mathcal{P}_{yu}\big(\hat{\Delta}_{\mathcal{P}}^{(j-1)}\big)u_o$ is computed via eq. (82). The Wiener filter (eqs. 87–89) is then applied to separate the individual disturbance contributions $\hat{n}^{(j)}$, $\hat{d}_i^{(j)}$, and $\hat{w}^{(j)}$. From these, refined spectral envelopes $\mathbf{\Phi}_n^{(j)}$, $\mathbf{\Phi}_{d_i}^{(j)}$, $\mathbf{\Phi}_w^{(j)}$ are estimated, and the output noise covariance $C_k^{(X,j)}$ is recomputed with the updated broadband noise model. The multisine amplitudes $A_{j,k}$ are then redesigned accordingly, and a new calibration experiment is performed to yield $\hat{\boldsymbol{\delta}}^{(j)}$.

The procedure converges when

$$\left\|\hat{\boldsymbol{\delta}}^{(j)} - \hat{\boldsymbol{\delta}}^{(j-1)}\right\| < \epsilon_\delta \qquad \text{and} \qquad \mathbf{\Phi}_{\xi}^{\text{model}} \approx \hat{\mathbf{\Phi}}_{\xi}^{\text{meas}},$$

i.e. when the parameter estimates have stabilised and the model-predicted composite disturbance spectrum is consistent with the one derived from telemetry.

Each iteration refines two coupled quantities: the parametric uncertainty set, which determines the transfer functions, and the disturbance spectral model, which determines the noise weighting in the FIM and the Wiener separation quality.

8 Conclusion

The central thesis of this paper is that spacecraft pointing performance cannot be rigorously verified by analysing the estimation and control loops in isolation. When the plant model carries parametric uncertainty in LFR form, the sensitivity functions governing knowledge and pointing errors are intrinsically coupled between the navigation filter and the control law. The separation principle, while structurally valid for any fixed plant realisation, does not extend to performance verification under parametric dispersion—a distinction with direct consequences for current AOCS practice.

To formalise this observation, a complete family of joint sensitivity functions has been derived for the general (biased) case that encompasses kinematic filtering architectures, together with the conditions

under which these reduce to the classical MIMO sensitivities via the control matching conditions (eqs.36-37). The analysis has revealed that sensor and actuator alignment errors act not merely as biases, as commonly treated, but as complex gain perturbations that reshape both the disk margins and the error budgets. The Bode integral limitation, extended here to the joint loop, further demonstrates that the placement of filter poles participates in the fundamental bandwidth–sensitivity trade-off alongside the controller poles.

Moving from analysis to validation, the paper has introduced a systematic framework for in-orbit identification of the LFR. The key enabler is the composite measurement disturbance ξ, which consolidates all unknown environmental inputs into a single observable quantity and determines the noise weighting in the experiment design. By constructing the Fisher Information Matrix in eq.62 from the LFR sensitivity gradients in eq.61, optimal multisine excitation signals can be designed that maximise parametric information content under spacecraft safety constraints. An exhaustive analysis of eight candidate injection points has identified five that are structurally independent, each exciting qualitatively distinct combinations of the joint sensitivity functions—ensuring that the resulting FIM is well conditioned across the parameter space.

The identified model, in turn, closes the verification loop: a frequency-domain Wiener filter separates individual disturbance contributions from operational telemetry, enabling reconstruction of the true knowledge and pointing errors with per-source budget decomposition. Worst-case bounds over the residual parametric uncertainty follow from μ-analysis, and an iterative refinement procedure progressively tightens both the parameter estimates and the disturbance characterisation until model and telemetry reach spectral consistency. Taken together, these results promote the LFR from a design-time abstraction to a flight-operational instrument. By feeding identified parameters and reconstructed disturbances back into the sensitivity functions derived here, pointing performance and robustness margins can be systematically verified—and improved—directly from commissioning data, bridging the gap between frequency-domain design tools and the time-domain Monte Carlo simulations that remain the prevailing verification approach in the industry.

Appendix A

In this Appendix it is proven that the sensitivity of an LFR,

$$\mathcal{F} = M_{\mathcal{F}_{22}} + M_{\mathcal{F}_{21}}\,\Delta_{\mathcal{F}}\left(I - M_{\mathcal{F}_{11}}\Delta_{\mathcal{F}}\right)^{-1} M_{\mathcal{F}_{12}}$$

with respect to a scalar uncertain parameter δ_i that may appear with repetitions on the diagonal of $\Delta_{\mathcal{F}}$ is

$$\frac{\partial \mathcal{F}}{\partial \delta_i} = \mathcal{R}_{L_{\mathcal{F}}}\, E_{\mathcal{F}_i}\, \mathcal{R}_{R_{\mathcal{F}}},$$

where $\mathcal{R}_{L_{\mathcal{F}}} = M_{\mathcal{F}_{21}}(I - \Delta_{\mathcal{F}}\, M_{\mathcal{F}_{11}})^{-1}$, $\mathcal{R}_{R_{\mathcal{F}}} = (I - M_{\mathcal{F}_{11}}\,\Delta_{\mathcal{F}})^{-1} M_{\mathcal{F}_{12}}$, and $E_{\mathcal{F}_i} = \partial\Delta_{\mathcal{F}}/\partial\delta_i$.

Define the right resolvent $R_R \triangleq (I - M_{11}\Delta)^{-1} M_{12}$, where for brevity we drop the subscript $\mathcal{F}$ and write M_{jk} for $M_{\mathcal{F}_{jk}}$ and Δ for $\Delta_{\mathcal{F}}$. Then

$$\mathcal{F} = M_{22} + M_{21}\,\Delta\, R_R.$$

Differentiating with respect to δ_i:

$$\frac{\partial \mathcal{F}}{\partial \delta_i} = M_{21}\, E_i\, R_R + M_{21}\,\Delta\,\frac{\partial R_R}{\partial \delta_i}, \tag{95}$$

where $E_i = \partial\Delta/\partial\delta_i$.

To compute $\partial R_R/\partial\delta_i$, apply the matrix-derivative identity $\partial A^{-1}/\partial x = -A^{-1}(\partial A/\partial x)A^{-1}$ to $A = I - M_{11}\Delta$:

$$\frac{\partial}{\partial \delta_i}\,(I - M_{11}\Delta)^{-1} = (I - M_{11}\Delta)^{-1}\, M_{11}\, E_i\, (I - M_{11}\Delta)^{-1}\,.$$

Hence

$$\frac{\partial R_R}{\partial \delta_i} = (I - M_{11}\Delta)^{-1}\, M_{11}\, E_i\, R_R. \tag{96}$$

Substituting eq.96 into eq.95:

$$\frac{\partial \mathcal{F}}{\partial \delta_i} = M_{21}\, E_i\, R_R + M_{21}\,\Delta\,(I - M_{11}\Delta)^{-1}\, M_{11}\, E_i\, R_R = M_{21}\left[I + \Delta\,(I - M_{11}\Delta)^{-1}\, M_{11}\right] E_i\, R_R.$$

It remains to show that the bracketed term equals $(I - \Delta\, M_{11})^{-1}$. Using the *push-through identity* $\Delta(I - M_{11}\Delta)^{-1} = (I - \Delta\, M_{11})^{-1}\Delta$, one obtains

$$\begin{aligned} I + \Delta\,(I - M_{11}\Delta)^{-1}\, M_{11} &= I + (I - \Delta\, M_{11})^{-1}\,\Delta\, M_{11} \\ &= (I - \Delta\, M_{11})^{-1}\left[(I - \Delta\, M_{11}) + \Delta\, M_{11}\right] \\ &= (I - \Delta\, M_{11})^{-1}\,. \end{aligned}$$

Therefore

$$\frac{\partial \mathcal{F}}{\partial \delta_i} = \underbrace{M_{21}\,(I - \Delta\, M_{11})^{-1}}_{\mathcal{R}_{L_{\mathcal{F}}}}\; E_i\; \underbrace{(I - M_{11}\,\Delta)^{-1}\, M_{12}}_{\mathcal{R}_{R_{\mathcal{F}}}} = \mathcal{R}_{L_{\mathcal{F}}}\, E_{\mathcal{F}_i}\, \mathcal{R}_{R_{\mathcal{F}}},$$

which completes the proof.

Acknowledgments

None.

Declaration of Use of Artificial Intelligence

Artificial intelligence was used to check notational consistency and grammar.

References

[1] Sigurd Skogestad and Ian Postlethwaite. *Multivariable feedback control: analysis and design*. John Wiley & Sons, 2005. ISBN: 978-0-470-01168-3.

[2] Jie Chen, Song Fang, and Hideaki Ishii. Fundamental limitations and intrinsic limits of feedback: An overview in an information age. *Annual Reviews in Control*, 47:155–177, 2019. doi: 10.1016/j.arcontrol.2019.03.011.

[3] Graham C Goodwin, David Q Mayne, and J Shim. Trade-offs in linear filter design. *Automatica*, 31(10):1367–1376, 1995. doi: 10.1016/0005-1098(95)00061-Z.

[4] Graham C Goodwin and María M Seron. Fundamental design tradeoffs in filtering, prediction, and smoothing. *IEEE transactions on automatic control*, 42(9):1240–1251, 1997. doi: 10.1109/9.623085.

[5] Maria M Seron, Julio H Braslavsky, and Graham C Goodwin. *Fundamental limitations in filtering and control*. Springer Science & Business Media, 2012. doi: 10.1007/978-1-4471-0965-5.

[6] Diego S Carrasco and Graham C Goodwin. Connecting filtering and control sensitivity functions. *Automatica*, 50(12):3319–3322, 2014. doi: 10.1016/j.automatica.2014.10.042.

[7] F Landis Markley, John Crassidis, and Yang Cheng. Nonlinear attitude filtering methods. In *AIAA guidance, navigation, and control conference and exhibit*, page 5927, 2005. doi: 10.2514/6.2005-5927, `https://doi.org/10.2514/6.2005-5927`.

[8] Ern J Lefferts, F Landis Markley, and Malcolm D Shuster. Kalman filtering for spacecraft attitude estimation. *Journal of Guidance, control, and Dynamics*, 5(5):417–429, 1982. doi: 10.2514/3.56190.

[9] F Landis Markley and John L Crassidis. *Fundamentals of Spacecraft Attitude Determination and Control*. Springer, 2014. doi: 10.1007/978-1-4939-0802-8.

[10] John L Crassidis, F Landis Markley, and Yang Cheng. Survey of nonlinear attitude estimation methods. *Journal of guidance, control, and dynamics*, 30(1):12–28, 2007. doi: 10.2514/1.22452.

[11] Mark E Pittelkau. Rotation vector in attitude estimation. *Journal of guidance, control, and dynamics*, 26(6):855–860, 2003. doi: 10.2514/2.6929.

[12] Mehmet Esit, Sirin Yakupoglu, and Halil Ersin Soken. Attitude filtering for nanosatellites: A comparison of different approaches under model uncertainties. *Advances in Space Research*, 68(6):2551–2564, 2021. doi: 10.1016/j.asr.2021.04.043.

[13] Yaguang Yang and Zhiqiang Zhou. Spacecraft dynamics should be considered in kalman filter attitude estimation. In *AAS/AIAA Space Flight Mechanics Meeting*, number NF1676L-22885, 2016.

[14] Wei-Min Lu, Kemin Zhou, and John C. Doyle. Stabilization of uncertain linear systems: An LFT approach. *IEEE Transactions on Automatic Control*, 41(1):50–65, 1996. doi: 10.1109/9.481607.

[15] Marc Hirth, Thomas Ott, Nicolas Deslaef, Bénédicte Girouart, Torsten Vogel, Martin Closs, Jennifer Campuzano San Miguel, Nicola Guercio, Nicolas Mosson, and Nils Neumann. P4com: Esa pointing error engineering for telecommunication missions. In *11th International ESA Conference on Guidance, Navigation and Control Systems*, 2021.

[16] Marc Hirth, Haifeng Su, Thomas Ott, Massimo Casasco, and Guillermo Ortega. Peet v1. 0: the state-of-the-art pointing and performance error engineering tool for space missions. In *10th International ESA Conference on Guidance, Navigation and Control Systems*, 2017.

[17] Ilham Courie, Francesco Sanfedino, and Daniel Alazard. Worst-case pointing performance analysis for large flexible spacecraft. *arXiv preprint arXiv:2106.01893*, 2021. doi: 10.48550/arXiv.2106.01893.

[18] M.G. Safonov. Feedback properties of multivariable systems: The role and use of the return difference matrix. *IEEE Trans. Automatic Control*, 26:47–65, 1981. doi: 10.1109/TAC.1981.1102566.

[19] James S Freudenberg, Christopher V Hollot, Richard H Middleton, and Varodom Toochinda. Fundamental design limitations of the general control configuration. *IEEE Transactions on Automatic Control*, 48(8):1355–1370, 2003. doi: 10.1109/TAC.2003.815017.

[20] Vinay Kariwala and Sigurd Skogestad. Limits of disturbance rejection for indirect control. In *Proceedings of the 44th IEEE Conference on Decision and Control*, pages 3620–3625. IEEE, 2005. doi: 10.1109/CDC.2005.1582724, https://doi.org/10.1109/CDC.2005.1582724.

[21] *ECSS - European Cooperation for Space Standardization, "Control Performance Guidelines", ECSS-E-HB-60-10A, 2010.*

[22] Peter Seiler, Andrew Packard, and Pascal Gahinet. An introduction to disk margins [lecture notes]. *IEEE Control Systems Magazine*, 40(5):78–95, 2020. doi: 10.1109/MCS.2020.3005277.

[23] Eugene Lavretsky and Kevin A Wise. Bode's integral theorem and flight control. *Journal of Guidance, Control, and Dynamics*, 48(5):982–990, 2025. doi: 10.2514/6.2024-0722.

[24] Daniel Alazard. *Reverse engineering in control design*. John Wiley & Sons, 2013. doi: 10.1002/9781118603932.

[25] Lennart Ljung et al. *System Identification: theory for the user*. Prentice-hall, Inc., 1987. ISBN: 978-0-136-56695-3.

[26] Torsten Söderström and Petre Stoica. *System identification*. Prentice-Hall, Inc., 1988. ISBN: 978-0-138-81236-2.

[27] Sergueï A Aïvazian, Igor S Enioukov, and Lev D Mechalkine. *Eléments de modélisation et traitement primaire des données*. Editions Mir, 1986.

[28] Steven M Kay. *Fundamentals of statistical signal processing: estimation theory*, volume 1. Prentice-Hall, Inc., 1993. ISBN: 978-0-133-45711-7.

[29] V.V. Federov. *Theory of Optimal Experiments*. Academic Press, Inc., 1972.

[30] Jack Kiefer. General equivalence theory for optimum designs (approximate theory). *The annals of Statistics*, pages 849–879, 1974. doi: 10.1214/aos/1176342810.

[31] Piotr Lichota, Krzysztof Sibilski, and Per Ohme. D-optimal simultaneous multistep excitations for aircraft parameter estimation. *Journal of Aircraft*, 54(2):747–758, 2017. doi: 10.2514/1.C033794.

[32] Patrick Guillaume, Johan Schoukens, Rik Pintelon, and Istvin Kollar. Crest-factor minimization using nonlinear chebyshev approximation methods. *IEEE transactions on instrumentation and measurement*, 40(6):982–989, 1991. doi: 10.1109/19.119778.

[33] Manfred Schroeder. Synthesis of low-peak-factor signals and binary sequences with low autocorrelation (corresp.). *IEEE transactions on Information Theory*, 16(1):85–89, 1970. doi: 10.1109/TIT.1970.1054411.